



A Journal of the Gesellschaft Deutscher Chemiker

Angewandte Chemie

GDCh

International Edition

www.angewandte.org

Accepted Article

Title: A Stable and Conductive Metallophthalocyanine Framework for Electrocatalytic Carbon Dioxide Reduction in Water

Authors: Donglin Jiang, Ning Huang, Ka Hung Lee, Stephan Irlé, Qihong Jiang, Yan Yue, and Xiaoyi Xu

This manuscript has been accepted after peer review and appears as an Accepted Article online prior to editing, proofing, and formal publication of the final Version of Record (VoR). This work is currently citable by using the Digital Object Identifier (DOI) given below. The VoR will be published online in Early View as soon as possible and may be different to this Accepted Article as a result of editing. Readers should obtain the VoR from the journal website shown below when it is published to ensure accuracy of information. The authors are responsible for the content of this Accepted Article.

To be cited as: *Angew. Chem. Int. Ed.* 10.1002/anie.202005274

Link to VoR: <https://doi.org/10.1002/anie.202005274>

RESEARCH ARTICLE

A Stable and Conductive Metallophthalocyanine Framework for Electrocatalytic Carbon Dioxide Reduction in Water

Ning Huang,^{[a],[b]} Ka Hung Lee,^{[c],[d]} Yan Yue,^[b] Xiaoyi Xu,^[b] Stefan Irle,^{[c],[d]} Qihong Jiang,^[a] and Donglin Jiang*^{[a],[e]}

[a] Prof. Dr. N. Huang, Dr. Q. Jiang, Prof. D. Jiang
Department of Chemistry, Faculty of Science
National University of Singapore,
3 Science Drive 3, Singapore 117543, Singapore
E-mail:

[b] Prof. Dr. N. Huang, Dr. Y. Yue, X. Xu
MOE Key Laboratory of Macromolecular Synthesis and Functionalization
State Key Laboratory of Silicon Materials, Department of Polymer Science and Engineering
Zhejiang University
Hangzhou 310027, China

[c] K. H. Lee, Prof. S. Irle
Bredesen Centre for Interdisciplinary Research and Graduate Education
University of Tennessee
Knoxville, TN 37996, U.S.A.

[d] Prof. S. Irle
Computational Sciences and Engineering Division & Chemical Sciences Division
Oak Ridge National Laboratory
Oak Ridge, TN 37831, U.S.A.

[e] Prof. D. Jiang
Joint School of National University of Singapore and Tianjin University
International Campus of Tianjin University
Binhai New City, Fuzhou 350207, China

Supporting information for this article is given via a link at the end of the document.

Abstract: Transformation of carbon dioxide to high value-added chemicals becomes a significant challenge for clean energy study. Here we developed a stable and conductive covalent organic framework for electrocatalytic carbon dioxide reduction to carbon monoxide in aqueous solution. The cobalt(II) phthalocyanine catalysts are topologically connected via robust phenazine linkage into two-dimensional tetragonal framework that is stable under boiling water, acid, or base conditions. The 2D lattice enables full π conjugation along x and y directions well as π conduction along the z axis across the π columns. With these structural features, the electrocatalytic framework exhibits a faradaic efficiency of 96%, an exceptional turnover number up to 320,000 and a long-term turnover frequency of $11,412 \text{ hour}^{-1}$, which is 32-fold increment compared to molecular catalyst. The combination of catalytic activity, selectivity, efficiency, and durability is desirable for clean energy production.

Introduction

The global climate change and energy demands underpin growing attention on exploring new technologies to convert carbon dioxide (CO_2) to carbon monoxide (CO) and other value-added chemicals.^[1] Electrochemical reduction of CO_2 is an ideal route to realize a carbon neutral clean energy. Progress over the past decade has greatly deepened our understanding of the electrochemical process involved in CO_2 reduction.^[2] An ideal electrocatalyst to pursuit is the one that could combine catalytic activity, selectivity, durability and availability in one material while catalytic activity relies on overpotential, current density, and turnover frequency and selectivity is determined by faradaic efficiency (FE). Remarkably, a wide range of materials ranging

from metals and their alloys to metal oxides and chalcogenides, metal-organic complexes, and carbon materials have been investigated for the electrocatalysis of CO_2 .^[2] For example, metal-organic complexes show much far superior turnover frequency to others. However, they suffer from drawbacks of tedious synthesis, high overpotential, and toxicity.^[2a] On the other hand, noble metals such as Au nanowires and Au-metal oxide hybrids promote the reaction at the lowest overpotential. However, the scarcity makes them unsuitable for application.^[2c,2d] Exploring an efficient electrocatalyst to combine activity (low overpotential high current density, and high turnover frequency) with selectivity, durability, and availability remains a substantial challenge.^[2]

We sought to explore highly stable catalytic materials by connecting molecular catalysts with robust covalent bond into two-dimensional covalent organic frameworks (2D COFs). Owing to the structural diversity, crystallinity, and porosity,^[3] COFs have been developed to show various functionalities, including semiconductors,^[4] light emitter,^[5] heterogeneous catalysis,^[6] adsorption and separation,^[7] and energy conversion.^[8] The unique structural features make COFs compelling candidates as catalysts for electrochemical CO_2 reduction.^[9] We rationalized that COFs could potentially achieve stability, conductivity, and catalytic activity for electrochemical CO_2 reduction: (1) The stability and durability can be achieved by using strong covalent bonds to connect catalytic sites into a robust framework, which cannot leak the catalytic sites; (2) the conductivity can be realized by using conjugated bonds to connect the catalytic sites and using tetragonal topology to create a fully π -conjugated network; (3) the catalytic activity and efficiency will be enhanced as electrons from electrodes can be smoothly transported to the reaction center via the shortest pathway in a highly conductive and ordered network.

RESEARCH ARTICLE

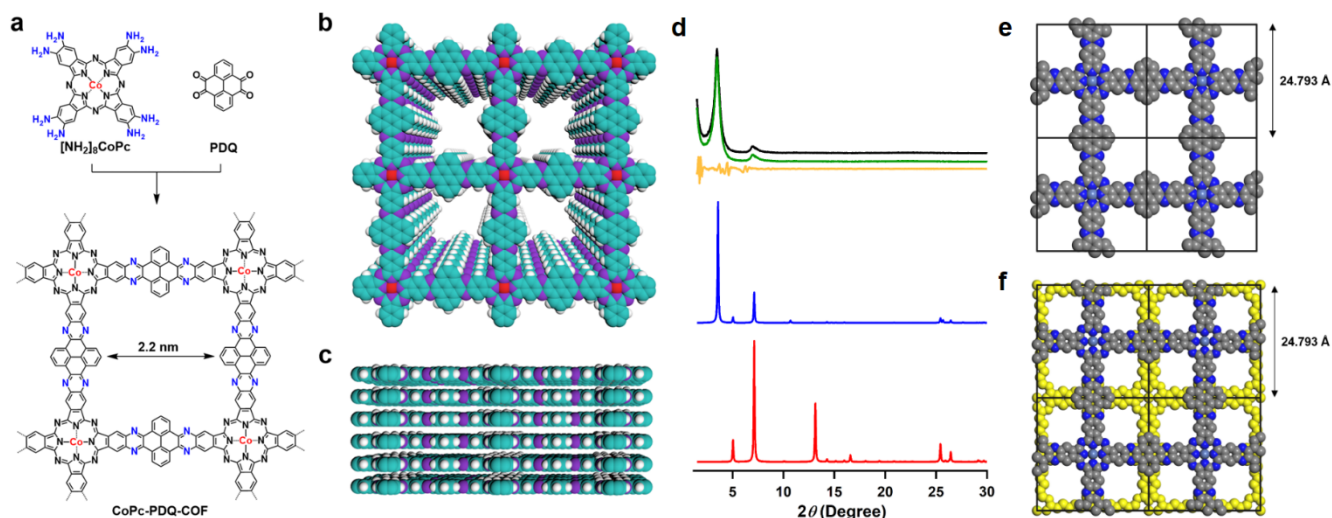


Figure 1. Design and synthesis of a conductive and stable electrocatalytic COF. a) Synthesis of CoPc-PDQ-COF with phenazine linkage by condensing $[\text{NH}_2]_8\text{CoPc}$ with PDQ. Reproduced crystal structure of (b) top and (c) side views of CoPc-PDQ-COF (purple, N; red, Co; green, C; white, hydrogen). d) Experimentally observed PXRD profiles of CoPc-PDQ-COF (black), Pawley refined profile (green) and their difference (orange), simulation results based on AA (blue) and AB (red) stacking manners. e) Reconstructed structure of CoPc-PDQ-COF in the AA stacking manner. f) Reconstructed structure of CoPc-PDQ-COF in the AB stacking manner.

However, fully exploring these structural features to design COFs-based electrocatalyst is still unprecedented.

Here we report a unique catalytic COF for electrochemical CO_2 reduction in water, by exploring the robust phenazine linkage to connect metallophthalocyanine catalytic sites into a fully π -conjugated lattice. The phenazine linkage is critical as it endows the resulting framework with stability and conductivity. It enables topological link of metallophthalocyanine knots at a regular distance of only 2.2 nm to form stacked tetragonal lattice. Therefore, the catalytic sites are fused to allow electron conduction along both the x and y axis while the π columns also facilitate the electron transfer along the z direction perpendicular to the 2D layer. With these structural features in one material, the resulting COF catalyst enables the combination of durability, conductivity, catalytic activity, and efficiency, which is hardly accessible with other molecular frameworks and amorphous polymers. We observed that it catalyzed the reduction of CO_2 to CO in water with high selectivity, exceptional turnover frequency, and long-term catalytic durability, which outperform most state-of-the-art solid-state and molecular electrocatalysts.^[1, 2, 6]

Results and Discussion

Design strategy. COFs have been synthesized by using different linkages ranging from boronate ester to imine and C=C bonds.^[3] Among various linkages, the phenazine ring is unique as it enables the use of π -conjugated ring to fuse knot and linker units into extended 2D π lattices.^[4a, 10] This linkage has two distinct features: one is the stability as the phenazine rings are fused and six-membered aromatic systems with exceptional chemical and thermal stabilities; another one is that it enables the design of fully π -conjugated lattice that is conductive. These structural advantages are hardly accessible with other linkages or other porous frameworks. To endow the phenazine-linked COFs with

high electrocatalytic activity, we selected metallophthalocyanines as knots, which are well known for electrocatalytic reduction of CO_2 . We designed the phenazine-linked metallophthalocyanine COF by using pyrene units as linkers, which can extend π conjugation along the x and y axis over the 2D sheets while the stacking layer structure offers the conduction along the z direction across the π columns, so that electrons directionally transport to catalytic sites over the shortest distance. Moreover, the built-in pores adsorb CO_2 and this adsorption shortens the electron transfer distance to CO_2 and facilitates the reduction reaction. This design strategy creates distinct interfaces that are key to the reduction of CO_2 as it combines durability, electric conductivity, catalytic activity, and selectivity in one catalyst.

Synthesis and characterization. The phenazine-linked metallophthalocyanine CoPc-PDQ-COF (Figure 1a–c) was synthesized by polycondensation of cobalt(II) 2,3,9,10,16,17,23,24-octakis(amino) phthalocyanine ($[\text{NH}_2]_8\text{CoPc}$) with 4,5,9,10-pyrenediquinone (PDQ) in a mixture of dimethylacetamide (DMAc) and ethylene glycol with acetic acid catalyst at 200 °C. After one week, CoPc-PDQ-COF was collected as shiny black powder in a yield of 85% (see Supporting Information). The crystalline structure of CoPc-PDQ-COF was resolved by PXRD analysis in combination with computational simulations. The CoPc-PDQ-COF exhibited high crystallinity with a series of strong PXRD peaks at 3.56°, 7.12°, 10.72°, and 25.84°, which were assigned to (100), (200), (300), and (001) facets, respectively (Figure 1d, black curve). Based on Scherrer equation, the crystallite size of CoPc-PDQ-COF was calculated to be 13.6 nm, which was smaller than an average size of 19.8 nm observed in electron microscopes. The tetragonal skeletons were simulated with density functional tight-binding (DFTB+) calculation to obtain optimum structure of layered lattice binding. Pawley refinement of experimental PXRD patterns verified the assignment of these diffraction peaks and exhibited good consistency with the observed PXRD patterns (Figure 1d, black curve), as confirmed

RESEARCH ARTICLE

by their inappreciable difference (Figure 1d, orange curve). Structural modeling using P4/M group space No. 83 with lattice parameters $\alpha = \beta = \gamma = 90$, $a = b = 24.793$ Å, and $c = 3.36$ Å gave a set of PXRD patterns (Figure 1d, green curve), which are in good accordance with the experimental data. The AA stacking lattice structure is illustrated in Figure 1e. On the contrary, a staggered lattice offset by the distance values of $a/2$ and $b/2$ (AB stacking, Figure 1f) cannot regenerate the experimental PXRD peaks (Figure 1d, blue curve). These results demonstrate that the condensation between $[\text{NH}_2]_6\text{CoPc}$ and PDQ forms CoPc-PDQ-COF with AA-stacked 2D layers. The PXRD peak at 25.84° reveals that CoPc-PDQ-COF is also ordered along the z axis with a short interlayer distance of 3.36 Å.

The CoPc-PDQ-COF was unambiguously characterized using various methods (Figures S1–S13). Fourier transform infrared (FT-IR) spectroscopy revealed the phenazine linkage formation with characteristic vibration peaks at $1,521$, $1,433$ and $1,354$ cm^{-1} . At the same time, the vibration bands of amino groups at $3,384$ and $3,313$ cm^{-1} and quinone units at $1,676$ cm^{-1} disappeared (Figure S1). Elemental analysis exhibited the contents of C, H, and N were 68.84%, 3.12%, and 18.79%, respectively, which were on the verge of the theoretical values of 71.17%, 2.99%, and 19.15%, respectively (Table S1). Inductively coupled plasma mass spectrometry revealed that the cobalt content was 4.35%, which was slightly lower than the theoretical value of 5.52%. Thermogravimetric analysis demonstrated that the CoPc-PDQ-COF did not lose weight even at 470 °C under nitrogen (Figure S2). Scanning electron microscopy (SEM) revealed bundles of belts, which extended to several tens of micrometers and are formed from elementary belt with high aspect ratios up to 35 and diameters of 12–44 nm (Figure 2a). High-resolution transmission electron microscopy (TEM) displayed that CoPc-PDQ-COF consisted of parallel arrays of 2D sheets with an intralayer distance of 3.5 Å (Figure 2b), which revealed a high order in its arrangement and was consistent with the (001) peak in PXRD patterns. Solid-state ^{13}C cross-polarization magic angle spinning nuclear magnetic resonance (CP/MAS NMR) spectroscopy revealed four characteristic signals at $\delta = 141.88$, 138.61 , 128.44 , and 126.25 ppm, which were attributable to the aromatic carbons of cobalt phthalocyanine knot (Figure S3). The signals at $\delta = 142.42$, 141.15 , 137.72 , 135.02 , and 131.64 ppm are assigned to the carbons on the pyrene linker (Figure S3). Solid-state electronic absorption spectroscopy revealed a wide band covering from ultraviolet regions to near infrared regions (Figure S4), suggesting an extended π cloud delocalization in the framework. Frontier molecular orbital calculation also demonstrated the delocalization of π electronic clouds over all the network (Figures S5–S9). In order to quantitatively measure the interlayer-stacking mode, we utilized the self-consistent charge DFTB method together with UFF (Universal Force Field) dispersion. Table S2 summarized the computational calculation results. The AA-stacking manner (atomic coordinates are listed in the Table S3) has single-layer stacking energy of 4.33 eV per lattice, which is much higher than that of the staggered AB manner (3.07 eV, atomic coordinates are given in Table S4).

The conductivity of CoPc-PDQ-COF was investigated by utilizing a four-point probe approach on a pressed 1.0 mm thick film. Notably, the bulk conductivity of CoPc-PDQ-COF was calculated up to 3.68×10^{-3} S m^{-1} at 298 K (Figure 2c, Table S5), which ranks as the highest one among all COF materials.^[3] The

activation energy was calculated to be 0.302 eV from the Arrhenius plot based on variable temperature current measurements (Figure 2c, inset). The high conductivity of CoPc-PDQ-COF originates from the fully π -conjugated yet stacked structure that allows electron transport over the whole skeleton.

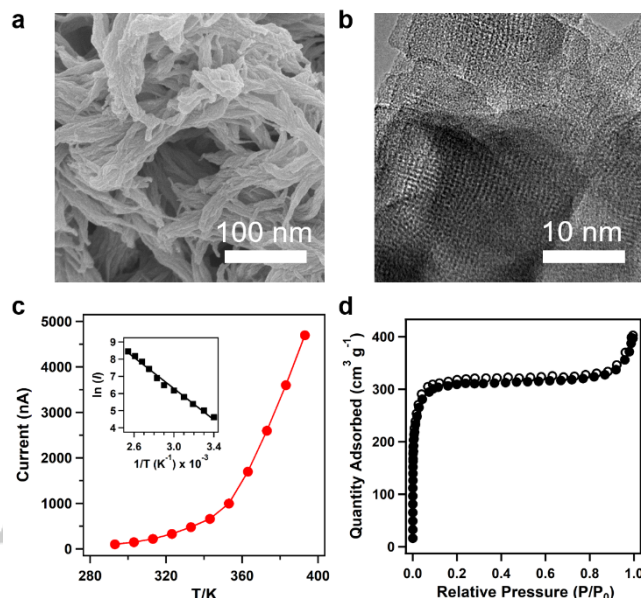


Figure 2. a) SEM images of CoPc-PDQ-COF at 100 nm scale bar. b) TEM image of CoPc-PDQ-COF. c) Temperature-dependent conductivity plot of CoPc-PDQ-COF pellet measured by a two-point probe at temperatures from 293 to 393 K with an applied voltage of 1 V. Inset shows the Arrhenius plot of the current versus temperature. d) Nitrogen sorption isotherm profile of CoPc-PDQ-COF measured at 77 K.

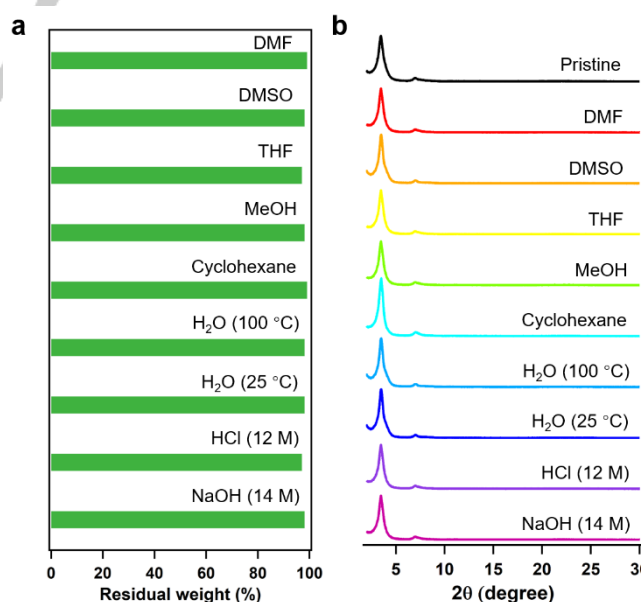


Figure 3. Chemical stability. a) Residual weight of CoPc-PDQ-COF after treatment in various solvents. Residual weight in DMF (99%), DMSO (98%), THF (97%), MeOH (98%), cyclohexane (99%), 25 °C water (98%), 100 °C water (98%), HCl (97%), and NaOH (98%). b) PXRD patterns of CoPc-PDQ-COF after 40-day treatment under different conditions.

RESEARCH ARTICLE

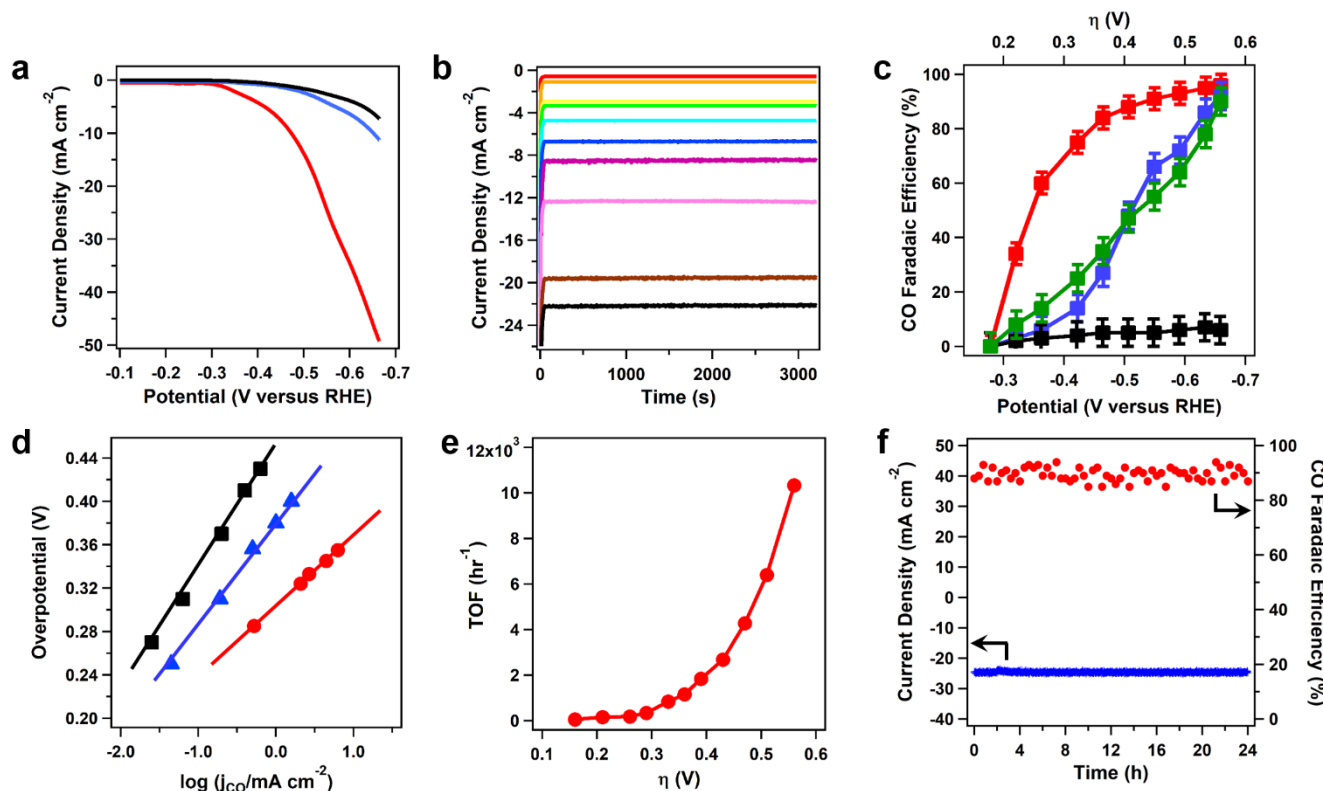


Figure 4. Electrochemical CO₂ reduction. a) LSV curves of CoPc-PDQ-COF (red curve), monomeric [NH₂]₆CoPc (blue curve), and commercial CoPc (black curve) in 0.5 M KHCO₃ solution saturated with CO₂. b) Chronoamperometric responses of CoPc-PDQ-COF at different potentials (red: -0.32 V; orange: -0.36 V; yellow: -0.43 V; green: -0.45 V; cyan: -0.49 V; blue: -0.54 V; purple: -0.58 V; pink: -0.61 V; brown: -0.65 V; black: -0.66 V). c) Faradaic efficiencies of CoPc-PDQ-COF (red curve), monomeric [NH₂]₆CoPc (blue curve), commercial CoPc (green curve), and carbon fiber (black curve). Error bars signify the standard deviation of three independent samples. d) Tafel plots of CoPc-PDQ-COF (red curve), monomeric [NH₂]₆CoPc (blue curve), and commercial CoPc (black curve). e) TOF of CoPc-PDQ-COF. f) Long-term operation stability of CoPc-PDQ-COF in current density (blue curve) and faradaic efficiency (red curve) over 24 h at -0.66 V ($\eta = 0.56$ V).

The CoPc-PDQ-COF possesses tetragonal channels with a theoretical diameter of 2.2 nm. The porosity property of the phenazine-linked COF was evaluated by the nitrogen sorption analysis at 77 K. As shown in Figure 2d, the sorption isotherm of CoPc-PDQ-COF was classified into typical type IV, which was characteristic in mesoporous materials. The Brunauer-Emmett-Teller (BET) surface area and pore volume values were calculated to be 762 m² g⁻¹ and 0.73 cm³ g⁻¹, respectively. Based on the nonlocal density functional theory model, the pore size distribution of CoPc-PDQ-COF was centered at 2.2 nm (Figure S10), which was highly close to the theoretical value. The surface area value of CoPc-PDQ-COF is similar with those of other phthalocyanine-based COFs, such as 2D-NiPc-BTDA COF,^[4b] NiPc COF,^[11a] and DZnPC-ANDI-COF.^[11b]

Chemical stability. Owing to the particularly chemical stability of phenazine linkage, the CoPc-PDQ-COF is exceptionally robust against various harsh conditions. To inspect the chemical robustness of CoPc-PDQ-COF, we soaked CoPc-PDQ-COF samples for 40 days in different solvents, including dimethylformamide (DMF), dimethyl sulfoxide (DMSO), tetrahydrofuran (THF), methanol (MeOH), cyclohexane, water (100 and 25 °C), concentrated HCl (12 M), and NaOH solution (14 M). Figure 3a shows the weight proportion of the residual COF samples. In aqueous solutions and organic solvents, CoPc-PDQ-COF showed little weight loss (< 4 wt%). Even under the ultra-harsh acid (concentrated HCl) or base (14 M NaOH) conditions, the residual weight proportion was as high as 97 wt% and 98 wt%,

respectively. In addition, the CoPc-PDQ-COF kept 98 wt% of its original weight after one-week hydrolysis in boiling water.

The CoPc-PDQ-COF retained its pristine crystalline network, as revealed by unchanged positions and intensities of its PXRD peaks after soaking in DMF, DMSO, THF, MeOH, cyclohexane, water (25 and 100 °C), NaOH solution (14 M), concentrated HCl (12 M) aqueous solutions for 40 days (Figure 3b). We assessed the crystallinity of above COF samples with its full width at half-maximum value of the (100) peak. Their width was calculated to be 100%, 99%, 100%, 99%, 100%, 100%, 99%, and 98% that of as-synthesized samples, respectively. These results indicate that the crystallinity of these COF samples is retained. The surface area values were 760, 759, and 762 m² g⁻¹ for the treated COF samples in boiling water, concentrated HCl (12 M), and aqueous NaOH solution (14 M) for 40 days, respectively (Figure S11); these values are in close proximity to that of freshly synthesized COF (762 m² g⁻¹). Moreover, the FT-IR spectra verified that these chemical bonds were preserved quite well (Figure S12). As far as we know, this phenazine-linked COF ranks as one of the most stable COFs to date.^[3] The stability originates from the robust phenazine ring that serves as the linkage to connect CoPc and PDQ consisting of stable phthalocyanine and pyrene backbones. Phenazine linkage has been widely used to construct stable heterocyclic polymers^[11c-11e] and COFs.^[4a,10,12d] Compared to other phenazine-linked analogue, CoPc-PDQ-COF decreases structural defects by improving crystallinity as evidenced by a

RESEARCH ARTICLE

narrow PXRD peak width. All these factors work together to enable an exceptional stability.

Electrocatalytic activity. The catalytic activity of CoPc-PDQ-COF was investigated in KHCO_3 aqueous solutions (0.5 M, pH = 7.2) saturated with CO_2 using a standard two-component electrochemical cell. The CoPc-PDQ-COF was thoroughly mixed with black carbon and dispersed in Nafion solution as binder to form a black homogeneous paste, and then coated on carbon fiber paper as a working electrode. In linear sweep voltammetry (LSV), CoPc-PDQ-COF exhibited a steep increase in reduction current density beyond -0.40 V based on a reversible hydrogen electrode (RHE), indicating a successful CO_2 reduction on CoPc-PDQ-COF (Figure 4a, red curve). The geometric cathodic current density reaches up to 49.4 mA cm^{-2} at -0.66 V (RHE, Figure 4a). In contrast, the monomeric $[\text{NH}_2]_8\text{CoPc}$ (Figure 4a, blue curve) and commercial CoPc (Figure 4a, black curve) exhibited much lower currents of only 7.2 and 11.2 mA cm^{-2} , respectively.

The time-dependent total geometric current density of CoPc-PDQ-COF was further estimated at different electrode potentials ranging from -0.32 to -0.66 V (Figure 4b). Notably, CoPc-PDQ-COF exhibited an excellent stability in the whole CO_2 reduction process under all the potentials. The reduction products were determined as CO and H_2 based on gas chromatography measurement. There is no other liquid products detected using nuclear magnetic resonance spectroscopy of the electrolyte. The electrochemical catalysis generated CO as the primary product, coincided with a small quantity of H_2 as a by-product. The faradaic efficiency for CO (FE_{CO}) was evaluated over the entire potential range (Figure 4c). The CO production was detected at a potential of -0.28 V (RHE) with a partial current density of 0.52 mA cm^{-2} . The FE_{CO} constantly increased with the upward overpotential and reached 60% at -0.36 V ($\eta = 260$ mV) and 96% at -0.66 V ($\eta = 560$ mV), respectively (Figure 4c, red curve). Remarkably, the FE_{CO} value of CoPc-PDQ-COF is higher than that of cobalt porphyrin COF-367-Co (53% at -0.67 V, $\eta = 560$ mV, Table S6)^[23]. Therefore, CoPc-PDQ-COF achieves an excellent selectivity as high as 96% in the electrochemical reduction of CO_2 into CO other than the reduction of water into H_2 , while COF-367-Co has a selectivity of only 53%. As control experiments, the FE_{CO} values of monomeric $[\text{NH}_2]_8\text{CoPc}$, commercial CoPc and carbon fiber were evaluated. The $[\text{NH}_2]_8\text{CoPc}$ (Figure 4c, blue curve) and CoPc (Figure 4c, green curve) exhibited a similar FE_{CO} with that of CoPc-PDQ-COF, while its performance was inferior, especially in the low overpotential range. The carbon fiber (Figure 4c, black curve) showed almost no electrocatalytic activity for CO_2 reduction, confirming that the catalytically active sites originate from the cobalt phthalocyanine units of CoPc-PDQ-COF.

To investigate the catalytic mechanism, we calculated the Tafel slope from a characteristic curve of the overpotential versus a logarithm of the steady partial current density of CO (Figure 4d). The linear Tafel slope was evaluated as $112 \text{ mV decade}^{-1}$ from 0.24 V to 0.42 V (Figure 4d, red curve). This result is consistent with other reported values, indicating that the formation of CO_2^- intermediate via electron transport from COF skeletons to CO_2 is the rate-determining step.^[12] Figure 5a shows the π structures of conductive CoPc-PDQ-COF and its catalytic cycle of electrochemical CO_2 reduction by cobalt phthalocyanine, which is also supported by CV measurements (Figure S13). Meanwhile, the monomeric $[\text{NH}_2]_8\text{CoPc}$ and commercial CoPc exhibited inferior Tafel slopes of $122 \text{ mV decade}^{-1}$ (Figure 4d, blue curve) and $125 \text{ mV decade}^{-1}$ (Figure 4d, black curve), respectively. The

small Tafel slope of CoPc-PDQ-COF compared to those of molecular catalysts indicates that less overpotential is required to get high current. These differences originate from the specific π structures of CoPc-PDQ-COF which consists of fully π conjugation along x and y axis and π conduction along the z direction, so that electrons are much easier to transport to the catalytic sites (Figure 5a). Notably, the surface concentration of electrocatalytically active CoPc species was calculated as high as 4.72% of total cobalt atoms by integrating the cyclic voltammetry peak area (Figure S12). This result is better than that (4%) of COF-367-Co,^[6f] indicating the high degree of accessibility to cobalt phthalocyanine active sites in the 2D CoPc-PDQ-COF.

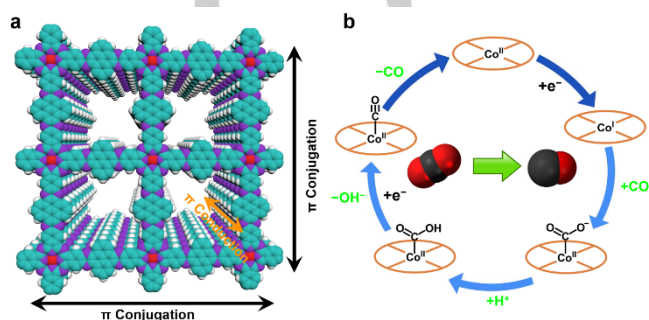


Figure 5. π structure of COF and catalytic cycle. a) The π structure of CoPc-PDQ-COF with π conjugation along the x and y axis and π conduction along the z axis which facilitate the electron transport to the cobalt(II) phthalocyanine catalytic centre. b) The electrocatalytic cycle of CO_2 reduction to CO by cobalt(II) phthalocyanine.

The specific activity of CoPc-PDQ-COF was quantified by standardizing the CO partial current density relative to the weight of active sites. The mass activity of CoPc-PDQ-COF was calculated up to 762 mA mg^{-1} at -0.66 V ($\eta = 0.56$ V). Furthermore, the turnover frequency (TOF) was evaluated given that all the cobalt active centers get involved in the reduction course of CO_2 . Notably, the TOF value for CO production was calculated as high as $11,412 \text{ h}^{-1}$ at $\eta = 0.56$ V (Figure 4e), while the turnover number reaches 320,000. These values are 32-fold as high as those of molecular catalyst $[\text{NH}_2]_8\text{CoPc}$. The TOF and turnover number of CoPc-PDQ-COF are superior to those ($9,396 \text{ h}^{-1}$ and 290,000 at $\eta = 0.55$ V) of imine-linked cobalt porphyrin COF-367-Co (1%), which is the best one reported to date.^[6f] Note that COF-367-Co (1%) specifically reduces the content of cobalt porphyrin sites in the framework to only 1% by diluting with inactive copper porphyrin, which raises the TOF value. Indeed, when the cobalt porphyrin content is 100%, the resulting COF-367-Co exhibits an average TOF of only 165 h^{-1} . Compared to CoPc-CN/CNT^[2a] and COF-367-Co,^[6f] CoPc-PDQ-COF achieves a much lower overpotential and a much higher current density. In comparison with other COFs, including TTF-Por(Co)-COF,^[13a] COF-Re₂Fe₂,^[2e] COF-366-F-Co,^[13b] COF-2,2'-bpy-Re,^[13c] and COF-300-AR,^[13d] CoPc-PDQ-COF^[2a] features the best overall performance. As shown in Table S6, CoPc-PDQ-COF surpasses the state-of-the-art organic and inorganic molecular catalysts including perfluorinated CoPc,^[14] nanoporous Ag,^[12c] Au nanowires,^[15a] and Pd nanoparticles.^[15b] Moreover, the CoPc-PDQ-COF catalyst exhibited much higher geometric current density than other catalysts under the same conditions (Table S6).

RESEARCH ARTICLE

Beside the catalytic activity, the lifetime and capability of repetitive use are key to high-performance electrocatalysis. The robust CoPc-PDQ-COF assumes a long-term catalytic durability. The chronoamperometric current density and Faradaic efficiency versus time were recorded over 24 h (Figure 4f). There was no significant loss in these two parameters. Notably, both the catalytic efficiency and selectivity retained the same values as the original ones. This is distinct from that of COF-366-Co, which has an initial TOF of 98 h^{-1} and further decreased to 56 h^{-1} after 24 h.^[6f] The remarkable long-term catalytic durability attributes to the stable yet fully π -conjugated structure, which produces high catalytic current densities. Moreover, the robust CoPc-PDQ-COF precludes the possibility of cobalt phthalocyanine detachment from the framework and thus boosts its performance stability.

To understand the CO_2 reduction process, we performed spin-polarized DFT calculations on single layer of CoPc-PDQ-COF. The results indicate that the two-electron involved CO_2 reduction is a two-step process; the first step is one-electron in involved transformation of CO_2 to COOH^* while the transformation from COOH^* to CO constitutes the second one-electron process (Figure S14). Their free energy change (ΔG) was determined to be -0.48 and -0.06 eV, respectively at 298 K. Subsequently, the anchored CO was spontaneously released from the COF surface with a ΔG value of -0.41 eV. Therefore, the first step is the rate-determining step, which is in accordance with the Tafel analysis. Its theoretical overpotential (η_i) was calculated to be 0.36 V. Moreover, we investigated the sequential proton-electron transfer processes for CO_2 reduction on CoPc-PDQ-COF (Figure S15). The valance change from Co(II) to Co(I) occurs in the first step upon the electron injection, which is mostly distributed on the $\text{Co-}d_{z^2}$ orbital and partly on the $\text{C-}p_z$ orbital of proximate carbons on Pc ring. The charge on the central Co(I) was $+0.87 |e|$, which was lower than $+1.17 |e|$ of Co(II). The formation of CO^{2-} anion was realized via a charge transfer ($0.55 |e|$) from Co(I) to the coordinated CO_2 molecule. The following formation of intermediate COOH^* involved the proton transfer. Finally, CO^* was generated from COOH^* through the concerted proton-electron transfer. As shown in Figure 5b, the periodic cycling between Co(II) and Co(I) promotes the conversion of CO_2 to CO.

Conclusion

In conclusion, we have explored a phenazine-linked stable and conductive metallophthalocyanine COF that catalyzes reduction of CO_2 to CO in water. This electrocatalyst is unique as it enables the full use of structural features of COFs to integrate full π conjugation, stable skeleton, and catalytic sites into one lattice, endowing the framework with stability, conductivity, and catalytic activity. The COF electrocatalyst achieves high efficiency and selectivity in catalyzing the reduction of CO_2 to CO with exceptional turnover number and frequency as well as long-term durability. This design strategy thus offers a platform based on 2D conjugated frameworks for tailoring robust yet well-defined catalysts to convert CO_2 into various valuable chemicals.

Acknowledgements

N.H. acknowledges support by the research start-up fund of Zhejiang University. K.H. was supported by an Energy Science

and Engineering Fellowship by the Bredesen Centre for Interdisciplinary Research and Graduate Education at the University of Tennessee, Knoxville. S.I. acknowledges support by the Laboratory Directed Research and Development (LDRD) Program of Oak Ridge National Laboratory. ORNL is managed by UT-Battelle, LLC, for DOE under contract DE-AC05-00OR22725. D.J. acknowledges supports by MOE tier 1 grant (R-143-000-A71-114) and NUS start-up grant (R-143-000-A28-133).

Conflict of interest

The authors declare no conflict of interest.

Keywords: covalent organic frameworks • 2D polymers • π conjugation • electrocatalysis • CO_2 reduction

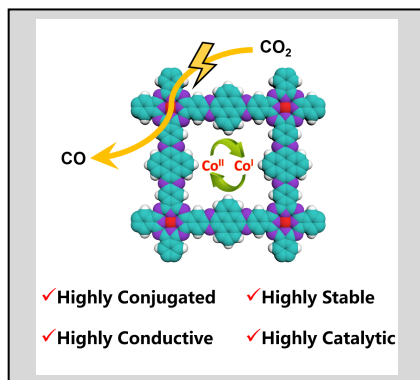
- [1] O. S. Bushuyev, P. Luna, C. T. Dinh, L. Tao, G. Saur, J. de Lagemaat, S. O. Kelley, E. H. Sargent, *Joule* **2018**, *2*, 825–832.
- [2] a) C. W. Machan, M. D. Sampson, C. P. Kubiak, *J. Am. Chem. Soc.* **2015**, *137*, 8564–8571; b) X. Zhang, Z. Wu, X. Zhang, L. Li, Y. Li, H. Xu, X. Li, X. Yu, Z. Zhang, Y. Liang, H. Wang, *Nat. Commun.* **2018**, *8*, 14675; c) W. L. Zhu, Y. J. Zhang, H. Y. Zhang, H. F. Lv, Q. Li, R. Michalsky, A. A. Peterson, S. H. Sun, *J. Am. Chem. Soc.* **2014**, *136*, 16132–16135; d) M. Ma, B. J. Trześniewski, J. Xie, W. A. Smith, *Angew. Chem. Int. Ed.* **2016**, *55*, 9748–9752; *Angew. Chem.* **2016**, *128*, 9900–9904; e) E. M. Johnson, R. Haiges, S. C. Marinescu, *ACS Appl. Mater. Interfaces* **2018**, *10*, 37919–37927; f) Z. W. Seh, J. Kibsgaard, C. F. Dickens, I. Chorkendorff, J. K. Nørskov, T. F. Jaramillo, *Science* **2017**, *355*, eaad4998; g) A. Y. Khodakov, W. Chu, P. Fongarland, *Chem. Rev.* **2007**, *107*, 1692–1744; h) D. Leckel, *Energy Fuels* **2009**, *23*, 2342–2358.
- [3] a) N. Huang, P. Wang, D. Jiang, *Nat. Rev. Mater.* **2016**, *1*, 16068; b) C. S. Diercks, O. M. Yaghi, *Science* **2017**, *355*, eaal1585; c) S.-Y. Ding, W. Wang, *Chem. Soc. Rev.* **2013**, *42*, 548–568; d) M. S. Lohse, T. Bein, *Adv. Funct. Mater.* **2018**, *28*, 1705553.
- [4] a) M. C. Wang, M. Ballabio, M. Wang, H.-H. Lin, B. P. Biswal, X. Han, S. Paasch, E. Brunner, P. Liu, M. Chen, M. Bonn, T. Heine, S. Zhou, E. Cánovas, R. Dong, X. Feng, *J. Am. Chem. Soc.* **2019**, *141*, 16810–16816; b) X. Ding, L. Chen, Y. Honsho, X. Feng, O. Saengsawang, J. Guo, A. Saeki, S. Seki, S. Irle, S. Nagase, V. Parasuk, D. Jiang, *J. Am. Chem. Soc.* **2011**, *133*, 14510–14513; c) D. D. Medina, T. Sick, T. Bein, *Adv. Energy Mater.* **2017**, *7*, 1700387; d) E. L. Spitzer, J. W. Colson, F. J. Uribe-Romo, A. R. Woll, M. R. Giovino, A. Saldivar, W. R. Dichtel, *Angew. Chem. Int. Ed.* **2012**, *51*, 2623–2627; *Angew. Chem.* **2012**, *124*, 2677–2681; e) S. Wan, J. Guo, J. Kim, H. Ihee, D. Jiang, *Angew. Chem. Int. Ed.* **2009**, *48*, 5439–5442; *Angew. Chem.* **2009**, *121*, 5547–5550; f) N. Huang, L. Zhai, D. E. Coupry, M. A. Addicoat, K. Okushita, K. Nishimura, T. Heine, D. Jiang, *Nat. Commun.* **2015**, *7*, 12325.
- [5] a) S. Dalapati, E. Jin, M. Addicoat, T. Heine, D. Jiang, *J. Am. Chem. Soc.* **2013**, *138*, 5797–5800; b) J. W. Crowe, L. A. Baldwin, P. L. McGrier, *J. Am. Chem. Soc.* **2016**, *138*, 10120–10123; c) Z. Li, A. M. Evans, I. Castano, M. J. Strauss, W. R. Dichtel, J.-L. Bredas, *J. Am. Chem. Soc.* **2018**, *140*, 12374–12377.
- [6] a) W. Cao, W. D. Wang, H.-S. Xu, I. V. Sergeev, J. Struppe, X. Wang, F. Mentink-Vigier, Z. Gan, M.-X. Xiao, L.-Y. Wang, G.-P. Chen, S.-Y. Ding, S. Bai, W. Wang, *J. Am. Chem. Soc.* **2018**, *140*, 6969–6977; b) Q. Sun, B. Aguila, J. Perman, N. Nguyen, S. Ma, *J. Am. Chem. Soc.* **2016**, *138*, 15790–15796; c) J. Zhang, X. Han, X. Wu, Y. Liu, Y. Cui, *J. Am. Chem. Soc.* **2017**, *139*, 8277–8285; d) H. Xu, J. Gao, D. Jiang, *Nat. Chem.* **2015**, *7*, 905–912; e) H. S. Xu, S.-Y. Ding, W. K. An, H. Wu, W. Wang, *J. Am. Chem. Soc.* **2016**, *138*, 11489–11492; f) S. Lin, C. S. Diercks, Y.-B. Zhang, N. Kornienko, E. M. Nichols, Y. Zhao, A. R. Paris, D. Kim, P. Yang, O. M. Yaghi, C. J. Chang, *Science* **2015**, *349*, 1208–1213; g) Y. Zhi, P. Shao, X. Feng, H. Xia, Y. Zhang, Z. Shi, Y. Mu, X. Liu, *J. Mater. Chem. A* **2018**, *6*, 374–382; h) Y. Zhang, Y. Hu, J. Zhao, E. Park, Y. Jin, Q. Liu, W. Zhang, *J. Mater. Chem. A* **2019**, *7*, 16364–16371.

RESEARCH ARTICLE

- [7] a) N. Huang, X. Chen, R. Krishna, D. Jiang, *Angew. Chem. Int. Ed.* **2015**, *54*, 2986–2990; *Angew. Chem.* **2015**, *129*, 3029–3033; b) N. Huang, R. Krishna, D. Jiang, *J. Am. Chem. Soc.* **2015**, *137*, 7079–7082; c) H. Fan, A. Mundstock, A. Feldhoff, A. Knebel, J. Gu, H. Meng, J. Caro, *J. Am. Chem. Soc.* **2018**, *140*, 10094–10098; d) S. Yuan, X. Li, J. Zhu, G. Zhang, P. V. Puyvelde, B. V. der Bruggen, *Chem. Soc. Rev.* **2019**, *48*, 2665–2681; e) H. Fan, J. Gu, H. Meng, A. Knebel, J. Caro, *Angew. Chem. Int. Ed.* **2018**, *57*, 4083–4087; *Angew. Chem.* **2018**, *130*, 4147–4151.
- [8] a) E. Jin, Z. Lan, Q. Jiang, K. Geng, G. Li, X. Wang, D. Jiang, *Chem* **2019**, *5*, 1632–1647; b) X. Wang, L. Chen, S. Y. Chong, M. A. Little, Y. Wu, W.-H. Zhu, R. Clowes, Y. Yan, M. A. Zwijnenburg, R. S. Sprick, A. I. Cooper, *Nat. Chem.* **2018**, *10*, 1180–1189; c) C.-Y. Lin, D. Zhang, Z. Zhao, Z. Xia, *Adv. Mater.* **2017**, *30*, 1703646; d) S. Haldar, K. Roy, R. Kushwaha, S. Ogale, R. Vaidhyanathan, *Adv. Energy Mater.* **2019**, 1902428; e) J. Zhao, P. Pachfule, S. Li, T. Langenhahn, M. Ye, C. Schlesiger, S. Praetz, J. Schmidt, A. Thomas, *J. Am. Chem. Soc.* **2019**, *141*, 6623–6630; f) T. Sick, A. G. Hufnagel, J. Kampmann, I. Kondofersky, M. Calik, J. M. Rotter, A. Evans, M. Döblinger, S. Herbert, K. Peters, D. Böhm, P. Knochel, D. D. Medina, D. Fattakhova-Rohlfing, T. Bein, *J. Am. Chem. Soc.* **2018**, *140*, 2085–2092; g) Y. Zhang, Y. Dong, J. Li, S. Li, P. Shao, X. Feng, B. Wang, *J. Am. Chem. Soc.* **2019**, *141*, 1923–1927.
- [9] D. Voiry, H. S. Shin, K. P. Loh, M. Chhowalla, *Nat. Rev. Chem.* **2018**, *2*, 0105.
- [10] a) J. Guo, Y. Xu, S. Jin, L. Chen, T. Kaji, Y. Honsho, M. A. Addicoat, J. Kim, A. Saeki, H. Ihee, S. Seki, S. Irlé, M. Hiramoto, J. Gao, D. Jiang, *Nat. Commun.* **2013**, *4*, 2736; b) V. A. Kuehl, J. Yin, P. H. H. Duong, B. Mastorovich, B. Newell, K. D. Li-Oakey, B. A. Parkinson, J. O. Hoberg, *J. Am. Chem. Soc.* **2018**, *140*, 18200–18207.
- [11] a) X. Ding, J. Guo, X. Feng, Y. Honsho, J. Guo, S. Seki, P. Maitarad, A. Saeki, S. Nagase, D. Jiang, *Angew. Chem. Int. Ed.* **2011**, *50*, 1289–1293; *Angew. Chem.* **2011**, *123*, 1325–1329; b) S. Jin, X. Ding, X. Feng, M. Supur, K. Furukawa, S. Takahashi, M. Addicoat, M. E. El-Khouly, T. Nakamura, S. Irlé, S. Fukuzumi, A. Nagai, D. Jiang, *Angew. Chem. Int. Ed.* **2013**, *52*, 2017–2021; *Angew. Chem.* **2013**, *125*, 2071–2075; c) C. Sun, F. Pan, H. Bin, J. Zhang, L. Xue, B. Qiu, Z. Wei, Z.-G. Zhang, Y. Li, *Nat. Commun.* **2018**, *9*, 743; d) S. Yang, M. Chu, Q. Miao, *J. Mater. Chem. C* **2018**, *6*, 3651–3657; e) J. Heiska, M. Nisula, M. Karppinen, *J. Mater. Chem. A* **2019**, *7*, 18735–18758.
- [12] a) S. Kapusta, N. Hackerman, *J. Electrochem. Soc.* **1984**, *131*, 1511–1514; b) J. Shen, R. Kortlever, R. Kas, Y. Y. Birdja, O. Diaz-Morales, Y. Kwon, I. Ledezma-Yanez, K. J. P. Schouten, G. Mul, M. T. M. Koper, *Nat. Commun.* **2015**, *6*, 8177; c) Q. Lu, J. Rosen, Y. Zhou, G. S. Hutchings, Y. C. Kimmel, J. G. Chen, F. Jiao, *Nat. Commun.* **2014**, *5*, 3242; d) Z. Meng, R. M. Stolz, K. A. Mirica, *J. Am. Chem. Soc.* **2019**, *141*, 11929–11937.
- [13] a) Q. Wu, R.-K. Xie, M.-J. Mao, G.-L. Chai, J.-D. Yi, S.-S. Zhao, Y.-B. Huang, R. Cao, *ACS Energy Lett.* **2020**, *5*, 1005–1012; b) D. A. Popov, J. M. Luna, N. M. Orchanian, R. Haiges, C. A. Downes, S. C. Marinescu, *Dalton Trans.* **2018**, *47*, 17450–17460; c) C. S. Diercks, S. Lin, N. Kornienko, E. A. Kapustin, E. M. Nichols, C. Zhu, Y. Zhao, C. J. Chang, O. M. Yaghi, *J. Am. Chem. Soc.* **2018**, *140*, 1116–1122; d) H. Liu, J. Chu, Z. Yin, X. Cai, L. Zhuang, H. Deng, *Chem* **2018**, *4*, 1696–1709
- [14] N. Morlanés, K. Takanabe, V. Rodionov, *ACS Catal.* **2016**, *6*, 3092–3095.
- [15] a) W. Zhu, W. Zhu, Y.-J. Zhang, H. Zhang, H. Lv, Q. Li, R. Michalsky, A. A. Peterson, S. Sun, *J. Am. Chem. Soc.* **2014**, *136*, 16132–16135; b) D. Gao, H. Zhou, J. Wang, S. Miao, F. Yang, G. Wang, J. Wang, X. Bao, *J. Am. Chem. Soc.* **2015**, *137*, 4288–4291.

RESEARCH ARTICLE

Entry for the Table of Contents



Pumping electrons to produce fuel. A fully π -conjugated 2D covalent organic framework with aligned metallophthalocyanine electrocatalytic sites enable electron pump to CO_2 reduction centers. The 2D π lattice catalyzes two electron reduction of CO_2 to CO in water to achieve an exceptional turnover number up to $320,000 \text{ hour}^{-1}$ and a faraday efficiency of 96%.

Institute and/or researcher Twitter usernames: chmjd@nus.edu.sg